

Simulations of cosmic ray feedback by AGN in galaxy clusters

Debora Sijacki^{1,2*}, Christoph Pfrommer³, Volker Springel¹ and Torsten A. Enßlin¹

¹*Max-Planck-Institut für Astrophysik, Karl-Schwarzschild-Straße 1, 85740 Garching bei München, Germany*

²*Institute of Astronomy, Madingley Road, Cambridge, CB3 0HA, United Kingdom*

³*Canadian Institute for Theoretical Astrophysics, University of Toronto, 60 St. George Street, Toronto, Ontario, M5S 3H8, Canada*

31 October 2018

ABSTRACT

Feedback processes by active galactic nuclei (AGN) appear to be a key for understanding the nature of the very X-ray luminous cool cores found in many clusters of galaxies. We investigate a numerical model for AGN feedback where for the first time a relativistic particle population in AGN-inflated bubbles is followed within a full cosmological context. In our high-resolution simulations of galaxy cluster formation, we assume that BH accretion is accompanied by energy feedback that occurs in two different modes, depending on the accretion rate itself. At high accretion rates, a small fraction of the radiated energy is coupled thermally to the gas surrounding the quasar, while in a low accretion state, mechanically efficient feedback in the form of hot, buoyant bubbles that are inflated by radio activity is considered. Unlike in previous work, we inject a non-thermal particle population of relativistic protons into the AGN bubbles, instead of adopting a purely thermal heating. We then follow the subsequent evolution of the cosmic ray (CR) plasma inside the bubbles, considering both its hydrodynamical interactions and dissipation processes relevant for the CR population. This permits us to analyze how CR bubbles impact the surrounding intracluster medium, and in particular, how this contrasts with the purely thermal case. Due to the different buoyancy of relativistic plasma and the comparatively long CR dissipation timescale we find substantial changes in the evolution of clusters as a result of CR feedback. In particular, the non-thermal population can provide significant pressure support in central cluster regions at low thermal temperatures, providing a natural explanation for the decreasing temperature profiles found in cool core clusters. At the same time, the morphologies of the bubbles and of the induced X-ray cavities show a striking similarity to observational findings. AGN feedback with CRs also proves efficient in regulating cluster cooling flows so that the total baryon fraction in stars becomes limited to realistic values of the order of $\sim 10\%$, more than a factor of 3 reduction compared with cosmological simulations that only consider radiative cooling and supernova feedback. We find that the partial CR support of the intracluster gas also affects the expected signal of the thermal Sunyaev-Zel'dovich effect, with typical modifications of the integrated Compton- y parameter within the virial radius of the order of $\sim 10\%$.

Key words: methods: numerical – black hole physics – cosmic rays – galaxies: clusters: general – cosmology: theory

1 INTRODUCTION

There is a growing body of observational evidence indicating that many galaxy clusters harbor in their centre supermassive black holes (BHs), which interact in a complex way

with their surroundings. Recently, spectacular images from the XMM-Newton and Chandra X-ray telescopes (e.g. McNamara et al., 2005; Fabian et al., 2006; Forman et al., 2007) have shed some light on this intricate interaction, showing clear imprints of central active galactic nuclei (AGN) in the intracluster medium of their host clusters. In particular, by comparing observations obtained at radio wavelengths

* E-mail: deboras@mpa-garching.mpg.de

with X-ray images, it is often seen that there are X-ray depressions in the innermost cluster regions which spatially correspond to significant radio emission (e.g. Owen et al., 2000; Blanton et al., 2001; Clarke et al., 2005). The most plausible candidate for inducing these features is the central BH, which is generating jet-inflated radio lobes, often simply dubbed ‘bubbles’.

There has been considerable theoretical effort to understand the interplay of AGN-driven bubbles with the intracluster medium (ICM) (e.g. Churazov et al., 2001; Quilis et al., 2001; Brüggén & Kaiser, 2002; Ruszkowski & Begelman, 2002; Dalla Vecchia et al., 2004; Omma et al., 2004; Sijacki & Springel, 2006a,b; Sijacki et al., 2007). Most of these studies have, for simplicity, considered bubbles that are filled with hot thermal gas, and by following their evolution with time, they tried to constrain how much heat AGN bubbles can deliver to the surrounding medium. However, the synchrotron and inverse Compton emission detected from the radio lobes suggests that they contain a significant amount of relativistic electrons and that they are permeated with magnetic fields. Besides relativistic electrons and magnetic fields, it is also very plausible that an important part of the pressure support in the bubbles stems from relativistic protons, especially if the AGN jets are heavy. To date it is however not clear, both from an observational and a theoretical point of view, what the precise composition of the bubbles, the relative mixture of hot gas, and non-thermal particle components really is. Also, we have no detailed knowledge about the strength and configuration of the magnetic fields within the bubbles.

Regarding the contribution from hot thermal gas, the work of Mazzotta et al. (2002) suggested that the bubble in the MKW 3s galaxy cluster may have a predominantly thermal origin, while Schmidt et al. (2002) found that in the Perseus cluster a thermal gas component cooler than ~ 11 keV filling the bubbles seems ruled out. Moreover, it is not clear whether entrainment of thermal gas by the radio jet is effective and how this should depend on the BH properties. A study of a larger sample of galaxy clusters with central X-ray cavities by Dunn et al. (2005) hints towards a rather complex picture, leaving several possibilities still open, both for significant pressure support by non-thermal protons or by hot thermal plasma, and for scenarios where the magnetic fields are filamentary at least in some of the cases.

Bearing in mind the outlined uncertainties it is still highly interesting to investigate the possible effects of cosmic rays (CRs) in AGN-inflated bubbles on cool core clusters, as considered already by several authors (e.g. Boehringer & Morfill, 1988; Loewenstein et al., 1991; Mathews & Brighenti, 2007; Guo & Oh, 2008; Sanders & Fabian, 2007; Ruszkowski et al., 2008). These studies have highlighted different channels of CR interaction with the thermal intracluster gas and have demonstrated that CRs can be dynamically important in galaxy clusters, contributing up to 50% of the central cluster pressure (but see Churazov et al. (2007) for somewhat lower estimates of CR pressure support of order of 10 – 20%). Nevertheless, due to the complicated nature of CR physics, most of these works were based on analytical or 1D numerical calculations, and neglected any cosmological evolution of the host clusters, and hence any possible dependence on its dynamical state. On the other hand, cosmological simulations of CRs produced at structure forma-

tion shocks by, for example, Miniati et al. (2001); Miniati (2002); Ryu et al. (2003); Ryu & Kang (2004) have highlighted the importance of a realistic cosmological setting for a more fateful generation, distribution and following evolution of CRs.

Recently, Enßlin et al. (2007) have proposed a simplified formalism for the treatment of CR protons that is suitable for implementation and use in self-consistent cosmological codes, as subsequently demonstrated by Jubelgas et al. (2008) and Pfrommer et al. (2006). In these numerical studies, the CR source processes considered were restricted to supernovae (SNe) and structure formation shock waves. While it was found that these CR sources can affect the interstellar medium of low mass galaxies significantly, they did not prevent the overcooling in the centres of galaxy groups and clusters. However, the possible impact of CR protons generated by central AGN has not been explored in these works, and this forms the primary objective of our current study.

This paper is organized as follows. In Section 2 we outline the methodology we have adopted to simulate CR bubbles and to follow their cosmological evolution. In Section 3, we present test runs performed for isolated halo simulations in order to analyze our numerical model in detail, while the bulk of our results from cosmological simulations of galaxy cluster formation is described in Section 4. Finally, we discuss our findings and draw our conclusions in Section 5.

2 METHODOLOGY

In this study we use an improved version of the massively parallel TreePM-SPH code GADGET-2 (Springel, 2005; Springel et al., 2001). The SPH formulation adopted in the code manifestly conserves both energy and entropy even in the presence of fully adaptive smoothing lengths, as implemented by Springel & Hernquist (2002). In addition to the gravity of dark matter and baryons, and to ordinary hydrodynamics, the code tracks radiative cooling of an optically thin plasma of hydrogen and helium, immersed in a time-varying, spatially uniform UV background (as in Katz et al., 1996). A subresolution multi-phase model for the ISM is used to follow star formation and supernovae feedback processes (Springel & Hernquist, 2003). Furthermore, we adopt the model for BH seeding and growth that has been suggested by Di Matteo et al. (2005) and Springel et al. (2005), modified however by the introduction of a second mode of AGN feedback to model radio activity, as described by Sijacki et al. (2007). These two modes are thermal heating from quasars at high BH accretion rates (BHARs), and mechanical feedback in the form of hot, buoyant bubbles occurring at low accretion rates.

In this study, we combine the AGN feedback prescription at low BHARs with a model for CR treatment that has been developed, implemented, and discussed by Enßlin et al. (2007), Jubelgas et al. (2008), and Pfrommer et al. (2006). This extension of our model allows us to account for a non-thermal component permeating the radio lobes. In this section, we outline the most important features of our combined BH and CR models, and we describe in detail the approximations we have adopted to model non-thermal particle populations in AGN-driven bubbles.

2.1 Black hole model

We represent BHs in the code by collisionless sink particles of initially very small mass, and we allow them to grow via gas accretion and through mergers with other BHs that happen to get sufficiently close. During the growth of structure, we seed every new dark matter halo above a certain mass threshold (e.g. $5 \times 10^{10} h^{-1} M_{\odot}$) with a central BH of mass $10^5 h^{-1} M_{\odot}$, provided the halo does not contain any BH yet. The seeding is accomplished on-the-fly by frequently invoking a parallel friends-of-friends algorithm. Once seeded, BHs can then grow by local gas accretion, with an accretion rate estimated with the Bondi-Hoyle-Lyttleton formula (Hoyle & Lyttleton, 1939; Bondi & Hoyle, 1944; Bondi, 1952). We impose a limit equal to the Eddington rate on the maximum allowed BHAR.

As for the BH feedback processes, we assume that they are composed of two physically distinct modes, depending on the BHAR itself. At high accretion rates, i.e. above 10^{-2} in Eddington units, we assume that the BH is in a radiatively efficient phase, where a small fraction of the bolometric accretion luminosity is coupled thermally to the local gas particles around the BH, with an efficiency of 5% and a spherical injection kernel. Instead, at low BHARs, we conjecture that the BH growth is characterized by a radiatively inefficient accretion flow, where most of the feedback is in a mechanical form, manifesting itself by hot buoyant bubbles that rise through the intragroup or intracluster medium. We relate the bubble energy content, radius and duty cycle with the BH physics, and adopt a somewhat higher efficiency of mechanical feedback of 20%. We note that Allen et al. (2006) recently showed that there exists a tight correlation between the Bondi accretion rates calculated based on observed gas temperature and gas density profiles and estimated BH masses, and the actual power emerging from these systems in relativistic jets. This lends observational support to our simple estimates of the BHARs.

2.2 CR implementation

We represent the CR population in each gaseous fluid element by a relativistic population of protons, which we approximately describe with an isotropic power-law distribution function in momentum space. In the simple formalism adopted here, this distribution function is fully defined by the power law slope α , its normalization C , and a dimensionless low momentum cut-off q : $dn/dp = Cp^{-\alpha}\theta(p-q)$. Here $\theta(x)$ denotes Heaviside step function and the dimensionless momenta are expressed in units of $m_p c$. We assume for clarity that the only source of CRs is given by the radiatively inefficient accretion mode of BHs, while we neglect other contributions from supernovae or particle acceleration at cosmic structure formation shocks, which have been extensively discussed in previous work (Jubelgas et al., 2008; Pfrommer et al., 2006, 2007, 2008; Pfrommer, 2008). We include CR loss processes in the form of thermalization by Coulomb interactions and losses due to hadronic interactions. We expect that within dilute bubbles these loss mechanisms should play a subdominant role compared to the pressure loss due to adiabatic expansion of the buoyantly rising bubbles. Therefore, we believe that our simulations also are representative, at least qualitatively, of the case of

a radio plasma that is dominated by a relativistic electron-positron population.

Even though in the present implementation of CR processes in GADGET-2, accounting for CR diffusion is in principle possible, in this study we refrain from trying to model it because this treatment of diffusion is only isotropic at present. Nevertheless, during the rise of a bubble, CR diffusion should be significantly suppressed perpendicular to the magnetic field lines that drape around the bubbles, only allowing CRs to diffuse efficiently in the wake of the bubbles (see e.g. Sanders & Fabian, 2007; Ruszkowski et al., 2008). Thus, isotropic CR diffusion would be a rather poor representation of this process, and neglecting diffusion altogether probably mimics the possible influence of magnetic draping effects with higher realism. Note, however, that the impact of magnetic fields on CR diffusion out of the bubbles is still poorly understood and is a matter of debate, hence a detailed treatment of this issue is beyond the scope of this work.

2.3 A model for CR bubbles

In the numerical framework we adopted for the description of CRs, we need to determine the power law slope α of the momentum spectrum representative for our system, its injection cut-off q_{inj} , and the fraction f_{CR} of the energy released by the BH that actually goes into the CRs. Once these values have been chosen we can follow the bubble's evolution and the loss processes of the CR component self-consistently, and compare with the case where the AGN-driven bubbles are purely thermal.

For the slope α we have tested values from 2.1 to 2.4, where a steeper power-law slope corresponds to a distribution with more low-energy CRs. These can thermalize faster and have a less relativistic equation of state that is closer to the 'harder' thermal case. We note that this range of values for the spectral slope is consistent with observational findings for the electron population in FRI sources, especially considering young systems (e.g. Birzan et al., 2004; Dunn et al., 2005). Similarly to the case in which CRs are produced by supernovae (Jubelgas et al., 2008) we establish the injection cut-off q_{inj} below which the CR energy is instantly thermalized. Equating the injection and loss time scale, we solve for the injection cut-off q_{inj} using equations (18) and (19) from Jubelgas et al. (2008) and by assuming an initial value of the intrinsic injection cut-off $q_{\text{init}} \sim 1$ for simplicity. Our results do not depend on a particular choice for q_{init} , provided $q_{\text{init}} \leq 1$ since Coulomb losses rapidly remove the low energy part of the CR spectrum, which gets almost instantly thermalized.

Finally, at a fixed mechanical feedback efficiency, we can choose whether to fill the AGN-inflated bubbles with relativistic gas exclusively, or to allow some of the hot thermal gas to permeate them as well, by regulating the parameter for the energy fraction going into CRs, f_{CR} . Note that, if Coulomb losses are important some fraction of initial energy delivered by AGN will be thermalized instantly as described above, such that f_{CR} can regulate only the remaining fraction of energy that in principle is available for injection into the CR population directly. So far there is no clear consensus in the observational literature (e.g. Mazzotta et al., 2002; Schmidt et al., 2002; Sanders & Fabian, 2007; Simionescu

et al., 2008) whether there is a significant thermal component inside radio bubbles or not, thus one of our main aims is to understand to what extent the numerical simulations predict noticeable changes in our results for different values of f_{CR} , which can provide interesting insights with respect to this question.

3 CR BUBBLES IN ISOLATED HALO SIMULATIONS

In this section we focus on idealized simulations of isolated galaxy clusters that harbour an AGN at their centre. The initial conditions for the runs consist of a gaseous cluster atmosphere in hydrodynamic equilibrium within a static NFW (Navarro et al., 1996, 1997) dark matter halo, as described in more detail in Sijacki & Springel (2006a). These systems are then evolved under the influence of radiative cooling, star formation, BH growth and different types of AGN feedback. The simplicity of these simulations relative to a full cosmological setting permits us to unambiguously identify the specific signatures of AGN-inflated bubbles that are filled with CRs, and to understand the differences that occur with respect to purely thermal bubbles.

3.1 Thermal versus CR content of bubbles

We start our analysis by considering a $10^{15} h^{-1} M_{\odot}$ halo where in regular time intervals of 10^8 yr a pair of spherical bubbles is injected into the innermost cluster region. We have fixed the energy content of the bubbles to be 2.5×10^{60} erg each, and the bubble radius to be $30 h^{-1}$ kpc. We have performed two identical runs, with the only difference being that in the first run the energy was injected as thermal energy into the bubbles, while in the second run the bubbles were filled with CRs instead.

In Figure 1, the panels from top to bottom show a time evolution sequence of this AGN-heated cluster. The panels on the left-hand side are projected temperature maps of the central cluster region for the case with thermal bubbles, while the panels of the middle column show the corresponding region in the run where the bubbles are filled with relativistic particles. To more clearly show the location of the CR bubbles, the panels on the right-hand side give the ratio of the projected CR pressure to the projected thermal pressure, so that regions that are permeated with a significant CR component can be clearly seen.

It is evident from this figure that the CRs modify both the bubble morphologies as well as their dynamics. The most striking difference in the temperature maps is that the CR bubbles actually appear as X-ray cavities, as has been observed in a number of clusters (e.g. Owen et al., 2000; Blanton et al., 2001; Nulsen et al., 2005; McNamara et al., 2005; Forman et al., 2007; Fabian et al., 2006). This is due to the fact that once the bubbles expand rapidly, their pressure drops more slowly than in the thermal case due to their softer equation of state, so that they become larger and thermally cooler*, as can be seen by comparing in the maps the

characteristic sizes of bubbles in the cases with thermal and CR injection. Thus, even though the bubble radius was the same at the moment of injection in both cases, the subsequent evolution leads to a marked difference in the size evolution of the bubbles.

Furthermore, the CR bubbles remain coherent for a significantly longer time than the thermal bubbles, and they reach larger cluster-centric distances as well. Support for this finding can be seen in the middle panels of Fig. 1, where the thermal bubbles that were still clearly defined in the top panel are already shredded when reaching a distance of $\sim 150 h^{-1}$ kpc, while the CR bubbles have risen to $\sim 200 h^{-1}$ kpc and are still intact at the same time. One reason for this behaviour lies in the significantly longer cooling time of the relativistic gas inside the bubbles compared with the thermal cooling time. Thus, while we injected initially the same energy in both runs, the CR bubbles preserve their entropy content for a longer time. Another reason lies in the enhanced buoyancy of the CR bubbles thanks to their larger size.

3.2 Self-regulated CR bubble heating

Now we turn to a more detailed analysis that involves a growing BH. To this end we introduce at the beginning of the simulations a seed BH of small mass at the centre in order to see how feedback by CR bubbles fares in establishing self-regulated AGN activity. These test runs are analogous to the ones presented in Sijacki et al. (2007), where a more detailed description of the set-up can be found. We also test variations of the CR power law slope from a value of 2.1 to 2.4, as illustrated in Figure 2, but we fix $q_{\text{init}} = 1$ and $f_{\text{CR}} = 1$.

First, we analyze the growth of the central BH as a function of time in the top panels of Figure 2. It can be seen that the CR bubbles lead to a self-regulated growth of the central BH similar to the thermal case, but at the end of the simulated time-span, the BH reaches a slightly smaller mass in the CR case. However, the detailed time evolution in the case of CR bubbles is physically more complex than in the thermal case. Initially, for $t < 0.1 t_{\text{Hubble}}$, the CR bubbles are less effective in heating the ICM, and consequently the central BH is growing more efficiently. During these early stages of BH growth, the average CR pressure in the cluster central region is smaller than the central pressure in the runs with thermal bubbles. Hence, during this early phase the combined effect of Coulomb and hadronic losses as well as the higher compressibility of composite CR plus thermal gas leads to a less efficient CR bubble feedback, as will be discussed in more detail in Section 3.3. However, even though this allows the gas to cool somewhat more efficiently towards the centre the amount of stars formed is roughly the same in the thermal and relativistic cases.

For $t > 0.1 t_{\text{Hubble}}$, the star formation rate begins to be more suppressed in the run with CR bubbles, because at this stage P_{CR} starts to be comparable to the local P_{th} . In

parable to the surrounding ICM particles to which we add non-thermal energy released by the AGN. This thermal component inside the bubbles is in most of the cases negligible with respect to the CR component.

* Note that prior to the CR injection into the bubble particles these have already by construction thermal energy content com-

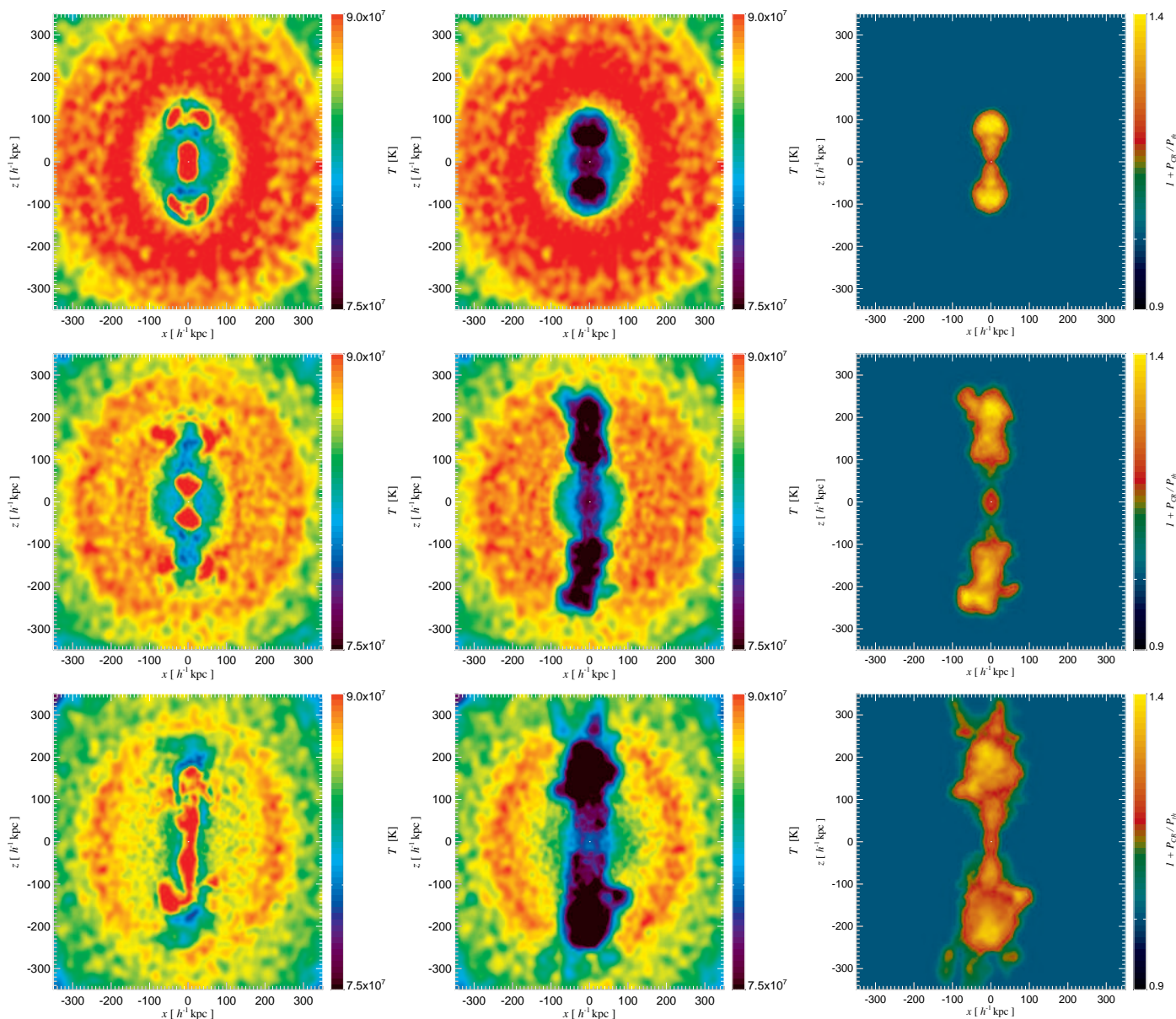


Figure 1. Projected mass-weighted temperature and pressure maps of the central cluster region at three different evolutionary stages, at times: $0.07 t_{\text{Hubble}}$ (top panels), $0.12 t_{\text{Hubble}}$ (middle panels), and $0.24 t_{\text{Hubble}}$ (bottom panels). The left-hand panels show temperature maps in the run where thermal bubbles have been injected in regular time intervals. The central panels illustrate a simulation where the bubbles were initially filled with relativistic particles instead. For this run, the regions where the CR pressure is significant with respect to the thermal pressure are shown in the right-hand panels. It can be clearly seen that the bubble dynamics, coherence and maximum cluster-centric distance reached are affected by the presence of a relativistic component filling the bubbles.

fact, for the run with $\alpha = 2.1$, this transition occurs somewhat earlier than in the simulation with a steeper α , given that for $\alpha = 2.1$ the cosmic ray pressure reaches significant values sooner. It can be seen that for $t > 0.1 t_{\text{Hubble}}$ the BHAR starts to oscillate dramatically as a consequence of the presence of a dominant relativistic particle component. A similar behaviour has been observed in the case of star formation in small dwarf galaxies in the work by Jubelgas et al. (2008). When a bubble is injected into the ICM and its P_{CR} is comparable or higher than the local P_{th} it will provide an extra pressure support to the ICM. While rising

buoyantly towards the cluster outskirts and heating the surrounding gas, this dramatically reduces the amount of gas that can be accreted by the central BH. Successively, CR pressure will get dissipated and gas will start to cool again leading to higher BHAR values, until another bubble is triggered, and the cycle is repeated. Note that at late times due to this behaviour of CR bubbles there is some residual star formation activity and the BH growth is not as efficiently terminated as it is the case for thermal bubbles.

The bottom panels of Figure 2 show how the profiles of gas density, temperature and entropy are affected by CR

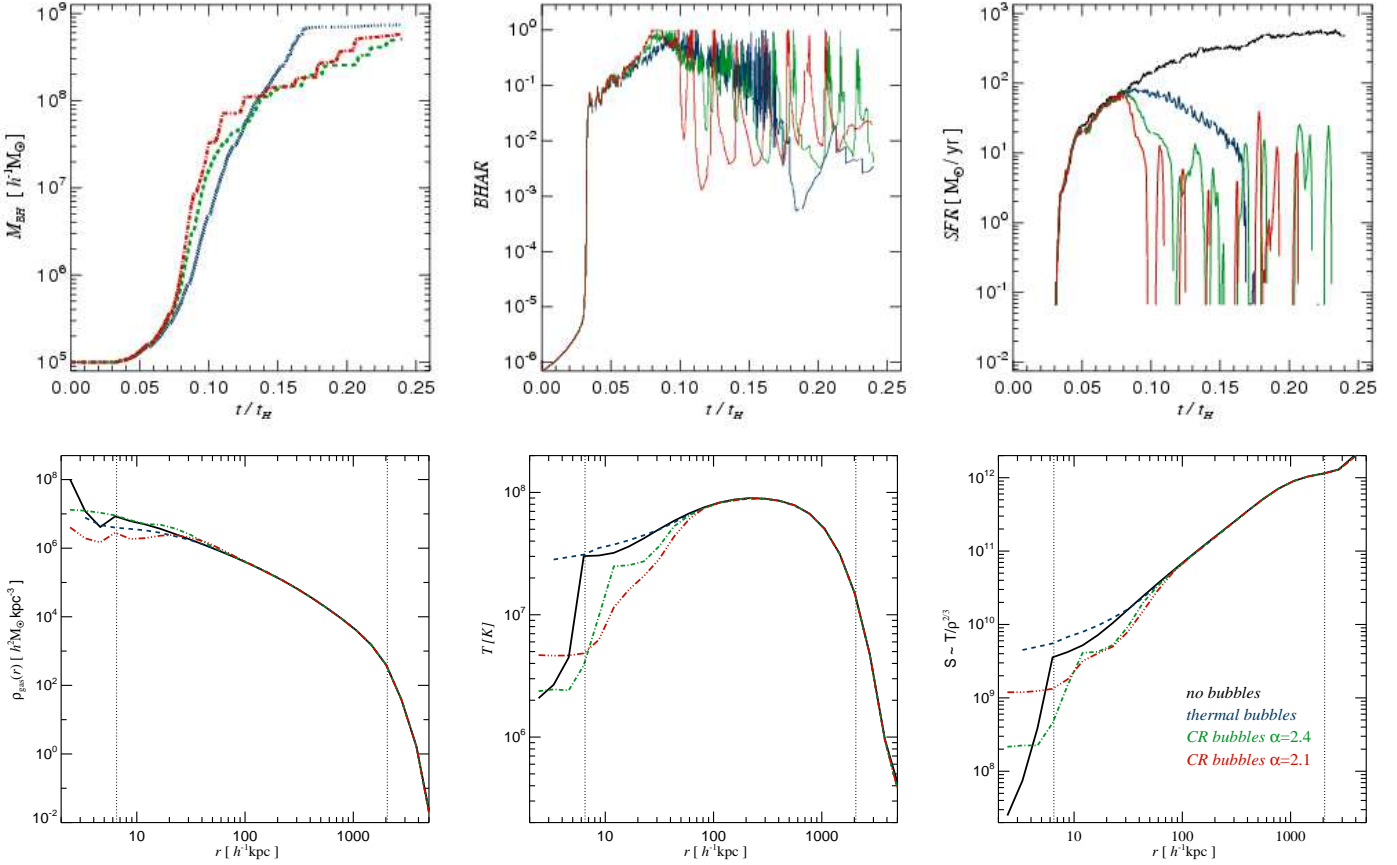


Figure 2. The top panels show the BH mass growth, BHAR in Eddington units, and star formation rate (SFR) as a function of time for four different runs: black lines denote the case with cooling and star formation only, blue lines show results where the AGN-driven bubbles are thermal, while the green and red lines refer to the case of CR bubbles. The run with a steeper spectral index of $\alpha = 2.4$ is represented with green lines, while the case of $\alpha = 2.1$ is drawn with red lines. The bottom panels show radial profiles of gas density, mass-weighted temperature, and entropy, for the same set of runs and with the same colour-coding. The vertical dotted lines denote the gravitational softening length and the virial radius of this halo.

bubbles. The radial temperature profile is always decreasing towards the central regions in the runs with CR bubbles, reflecting the fact that a significant fraction of non-thermal pressure builds up there. However, the gas density can either be increased or reduced relative to the thermal case, depending on whether P_{CR} is higher than P_{th} at a given instant. Finally, the gas entropy is also somewhat reduced in the innermost regions, mainly being driven by the variations in temperature. Overall, the simulation with a flatter CR spectrum shows a more significant imprint of CRs on the ICM, as expected due to the more pronounced high-energy tail of the CR momentum distribution, so that a significant level of P_{CR} can be maintained for a longer time interval.

3.3 Importance of Coulomb and hadronic losses

There are two primary dissipation processes for the CR particle population. One is given by individual electron scatterings in the Coulomb fields of CR particles and by small momentum transfers through excitations of plasma oscillations, which is especially efficient in the low momentum tail of the CR population (Gould, 1972). The other important CR energy loss process is due to inelastic collisions of CRs

on nucleons, where hadronic interactions produce pions that are then ultimately dissipated into radiation as well as thermal heat (e.g. Enßlin et al., 2007). Additionally, the process of MHD wave-mediated cosmic-ray heating (Loewenstein et al., 1991) could be relevant for the CR particle population within the bubbles (see e.g. Guo & Oh, 2008), that we do not consider in this work.

In order to gauge the relative importance of these loss processes we have performed two additional test runs where we have switched off CR losses altogether, or alternatively only allowed for Coulomb cooling. Based on these runs we find that in the case where bubbles are filled exclusively with CRs and where no diffusion is allowed, hadronic losses are not very important during the whole simulated timespan.

Instead, we find that Coulomb cooling is especially important in the early phases of BH growth. Here the Coulomb cooling time of the injected CR particles turns out to be rather short such that the CR energy is quickly thermalized into the ICM. Thus, in the run where only Coulomb cooling is allowed the BH is accreting mass as efficiently in the beginning as in the case with thermal feedback. However, for $t > 0.1 t_{\text{Hubble}}$, the CR pressure inside of the bubbles builds up and the characteristic time of Coulomb losses increases. As a result, the CRs thermalize very little of their

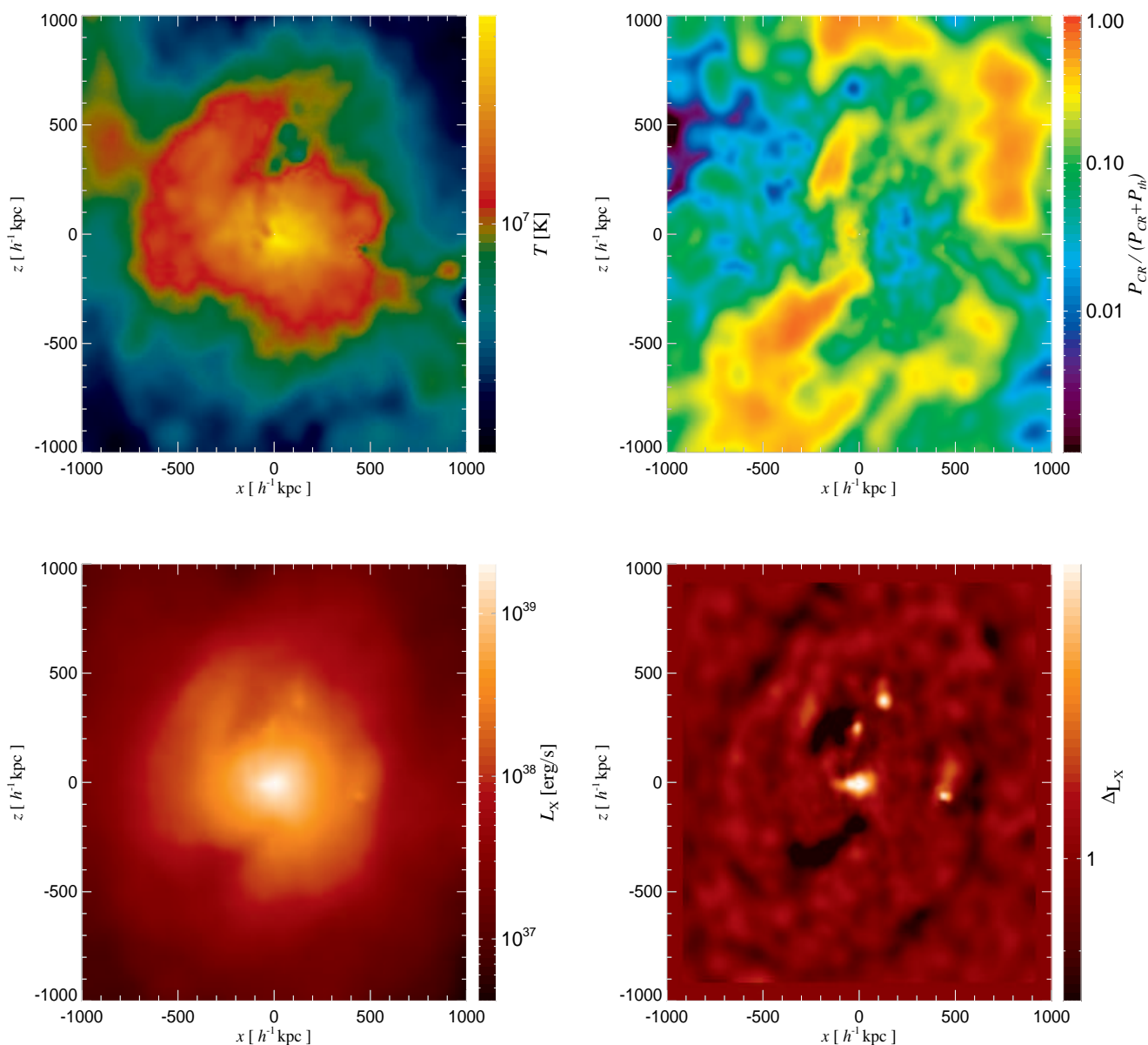


Figure 3. Maps of the central region of the *g676* galaxy cluster at $z = 0.1$. In the upper row, a mass-weighted temperature map is shown in the left-hand panel, while the right-hand panel illustrates the mass-weighted spatial distribution of P_{CR} relative to the total pressure. In the lower row, X-ray luminosity maps are illustrated. The right-hand panel gives an unsharp masked luminosity map, allowing for easier bubble identification.

energy content for $t > 0.15 t_{\text{Hubble}}$. Interestingly, in the case where no losses were allowed for the non-thermal population BH growth is somewhat faster during the very first part of the simulation than in the case of thermal bubbles. Here, CRs cannot thermalize part of their energy into the surrounding ICM and heat it, and since the composite of non-thermal and thermal pressure is more compressible, AGN feedback becomes somewhat less efficient than the purely thermal bubbles in the early stages of BH growth.

We have further explored the case where only one part of the available mechanical energy is delivered into CRs, while the other remained in thermal form. For values of f_{CR} as low as 0.1, the influence of CRs is barely distinguishable

from the purely thermal case. However, if we select f_{CR} of order of 0.5 or higher the composite of CRs plus thermal gas in the bubbles shows interesting properties. In particular, for $t < 0.1 t_{\text{Hubble}}$, the non-thermal component inside of the bubbles only weakly increases the gas compressibility, and these composite bubbles essentially behave as pure thermal bubbles. On the other hand, for $t > 0.1 t_{\text{Hubble}}$, the cosmic ray pressure P_{CR} inside of the composite bubbles reaches high values, so that CR processes become much more relevant. At this stage, the properties of composite bubbles and their feedback effects become very similar to the case of pure CR bubbles.

4 COSMIC RAY BUBBLES IN SIMULATIONS OF CLUSTER FORMATION

In this section we consider self-consistent cosmological simulations of galaxy cluster formation subject to AGN heating. From a cosmological box of size $479 h^{-1}\text{Mpc}$ on a side that has been evolved adopting a ΛCDM cosmology (Yoshida et al., 2001; Jenkins et al., 2001), a galaxy cluster with a mass of $\sim 10^{14} h^{-1}M_{\odot}$ has been selected (the ‘g676’ cluster), that is fairly relaxed at the present epoch. Using the Zoomed Initial Condition (ZIC) technique (Tormen et al., 1997), new initial conditions for this cluster have been constructed by resampling its Lagrangian region at a higher numerical resolution (Dolag, 2004). In Sijacki et al. (2007), we have presented several simulations of this cluster with different physics, including runs with cooling and star formation processes only, as well as simulations that analyzed the impact of our AGN feedback model with thermal bubbles. Here, we discuss analogous simulations that focus on the role of CRs in AGN-inflated bubbles. Further details about the numerical setup can be found in Sijacki et al. (2007). In our new simulations, we keep all numerical parameter choices (like gravitational softening lengths, number of SPH smoothing neighbours, etc.) exactly the same in order to clearly pin down the impact of the non-thermal nature of the bubbles.

4.1 Signatures of CR bubbles

We start our analysis by trying to identify a link between the CR bubble properties and specific features they induce in the ICM. In Figure 3, we show the central region of our most massive cluster at $z = 0.1$. The thickness of the projection slice is $300 h^{-1}\text{kpc}$, and the different panels give the projected mass-weighted temperature map (upper left-hand panel), the P_{CR} -to-total pressure ratio (upper right-hand panel), the X-ray luminosity map (lower left-hand panel) and an unsharp masked luminosity map (lower right-hand panel). The unsharp masked luminosity map has been produced by dividing the original luminosity map by a version of it that has been smoothed on $\sim 180 h^{-1}\text{kpc}$ scale. In the upper right-hand panel, the position of CR bubbles can be clearly identified. In the very centre of the cluster there is significant cosmic ray pressure, corresponding to very recent BH activity which is producing two small bubbles. Moreover, upwards from the central region there is a large plume filled with CR protons extending from $\sim 200 h^{-1}\text{kpc}$ to $\sim 500 h^{-1}\text{kpc}$ along the z -axis. Yet another plume is clearly visible in the lower region, propagating towards the lower-left corner, and having a total length of more than $\sim 200 h^{-1}\text{kpc}$. The temperature map reveals asymmetries along the direction of big CR plumes, and a close correspondence to the central small bubbles, where the temperature is somewhat reduced. However, it is in the luminosity maps that one can clearly identify CR bubbles, as depression regions in X-ray emissivity. The bubble morphologies and the reduction in X-ray emissivity in the regions that are permeated with CR particles are in very good qualitative agreement with a number of observational findings (e.g. Owen et al., 2000; Nulsen et al., 2005; Forman et al., 2007; Sanders & Fabian, 2007), suggesting that the presence of a non-thermal component inside of the bubbles is essential for

more faithful reproduction of the observational results and their understanding.

In Figure 4, we analyze the CR bubble morphologies at different cosmic times. To this end we plot the projected CR energy per unit mass in the x - z plane within a cubic box of size $4000 h^{-1}\text{kpc}$ on a side, at three different redshifts, $z = 1.0, 0.6$ and 0.2 . The left-hand panels refer to the run performed with $\alpha = 2.1$, while the right-hand panels are for $\alpha = 2.4$. The black dots over-plotted on the maps mark the positions of BH particles more massive than $1.5 \times 10^7 h^{-1}M_{\odot}$. Note that we have deliberately chosen not to vary the injection axis of the bubbles with time (which is always along the z -axis). This has been done in order to assess to what extent environmental effects like bulk motions, local overdensity fluctuations, or merger events, can displace bubbles from their initial injection position. At the first glance it can be noticed that the evolved CR bubble morphologies are rather complex, clearly lacking a strong axial symmetry, even though they were injected in a symmetric fashion. This emphasizes the important role played by the cosmological environment in modifying the bubble shapes.

The three epochs shown in Fig. 4 have been selected such that they correspond to merging events of the central BH with a smaller mass BH that once belonged to a satellite halo. Thus, at these epochs, the BH activity in the central region is rather vigorous, and several bubble episodes can be seen, from the central ones that are just injected, to the more peripheral ones which have risen and are now detached, but still have significant pressure support from CR protons. Interestingly, at $z = 1.0$, in the vicinity of the most massive cluster in the lower-right part, there is a smaller halo containing a central massive BH which during a similar time span has also generated two bubbles. At $z = 0.6$ this smaller halo reaches $\sim 1/3$ of the central cluster mass and merges with it violently. The central BHs of these halos merge as well, increasing the mass of the most massive BH by $\sim 10^9 h^{-1}M_{\odot}$. It can be seen that during this merger event the relic CR bubbles are significantly perturbed and displaced towards the right, in the direction from which the smaller halo was falling in.

Finally, by comparing the left-hand panels to the right-hand panels in Fig. 4, it can be seen that CR bubbles with a steeper power-law spectrum have in general similar morphologies to the $\alpha = 2.1$ case, but they show a somewhat smaller size and shorter survival time, as expected given that Coulomb losses become more important for a steeper spectrum.

4.2 Impact of CR bubbles on their host haloes

4.2.1 Radial profiles

In Figure 5, we show radial profiles of gas density (first row), mass-weighted temperature (second row), entropy (third row), and thermal pressure (last row) at three different epochs, $z = 0.5, 0.2$ and 0.0 . The black continuous lines are for the run with cooling and star formation only, blue dashed lines denote the run with thermal bubbles (as in Sijacki et al., 2007), while the green dot-dashed ($\alpha = 2.4$) and red triple dot-dashed lines ($\alpha = 2.1$) show the case with CR bubbles. It can be seen that the gas density is

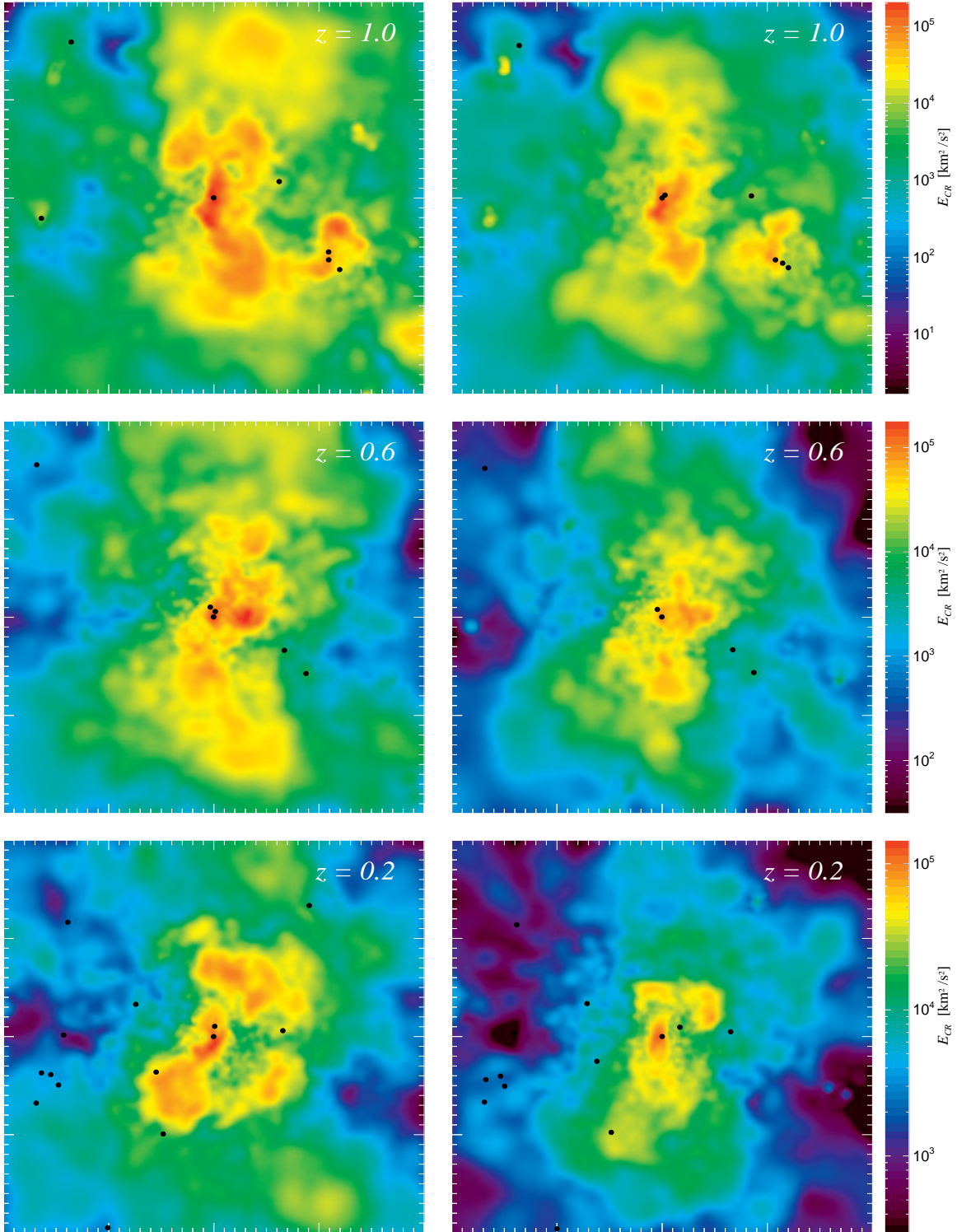


Figure 4. Projected mass-weighted CR energy per unit mass in boxes of $4000 h^{-1} \text{kpc}$ on a side at three different redshifts: $z = 1.0$ (top), 0.6 (middle) and 0.2 (bottom). The left-hand panels are for the run with $\alpha = 2.1$, while the right-hand panels show the case of $\alpha = 2.4$. The selected redshifts correspond to highly perturbed states of the cluster when it is undergoing merging events. It can be seen how environmental effects influence the morphologies and dynamics of CR bubbles.

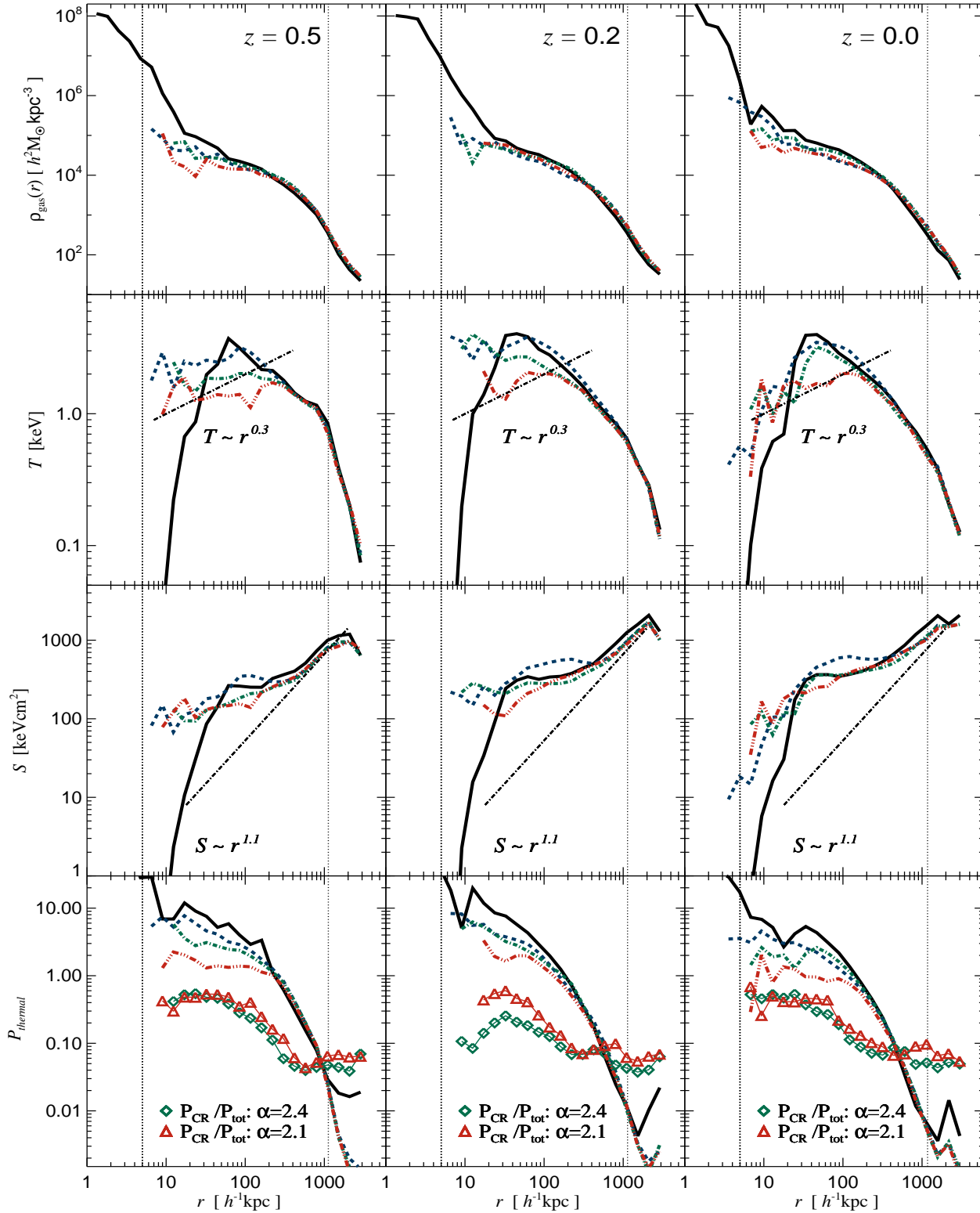


Figure 5. Radial profiles of gas density (first row), mass-weighted temperature (second row), entropy (third row) and thermal pressure (last row, in internal code units) of the g676 galaxy cluster at $z = 0.5$, 0.2 and 0.0 , respectively. Solid black lines illustrate the case without AGN heating. The dashed blue lines are for simulations where AGN feedback is included with purely thermal bubbles, as in Sijacki et al. (2007). The runs with CR filled bubbles are represented with green dot-dashed lines and red triple dot-dashed lines, for spectral indices of $\alpha = 2.4$ and $\alpha = 2.1$, respectively. The vertical dotted lines denote the gravitational softening length and the virial radius of this cluster. The dash-dotted lines in the second row of panels show the slope of the central temperature profiles of the cool core clusters found by Sanderson et al. (2006), while the dash-dotted lines in the third row illustrate the entropy scaling with radius, i.e. $S \propto r^{1.1}$. In the last row we also indicate the mean ratio of CR-to-total pressure in each bin, which is shown with green diamonds ($\alpha = 2.4$) and red triangles ($\alpha = 2.1$).

affected by the presence of relativistic particles in the bubbles, being roughly comparable to the simulation where the bubbles are purely thermal. However, the gas temperature is altered substantially and in general is always reduced in central regions, as we have also found for our isolated cluster simulations. This is simply caused by the fact that significant pressure support in the central cluster regions is in a non-thermal form, which decreases the thermal pressure needed to counteract the gravity exerted by the cluster's potential. In Sijacki et al. (2007) we have already shown that a self-regulated AGN feedback mechanism is required in order to obtain realistic temperature profiles that can reproduce the decline towards the innermost regions that has been observed in a number of cool core clusters. Having a significant population of non-thermal particles in the central bubbles further helps in this respect, and provides a natural explanation for the observed shape of the temperature profiles. Thus, the presence of a relativistic particle population inside AGN-inflated bubbles is not only essential for reproducing the observed morphologies of bubbles and X-ray cavities in the hot ICM, but it also improves the temperature distribution of the simulated galaxy clusters. However, our results also show that the AGN feedback efficiency and the assumed fraction of the energy in high energy CR protons are to a certain extent degenerate, suggesting that a detailed comparison with observations is needed to constrain both of these parameters individually.

The CR bubble feedback also steepens the entropy profile and brings it into closer agreement with X-ray observations, especially at intermediate radii from $\sim 20 h^{-1} \text{kpc}$ to $\sim 300 h^{-1} \text{kpc}$. Further information about the role of CR bubbles can be obtained from the last row of panels in Figure 5, where we plot radial profiles of the mass-weighted thermal pressure for all the runs we performed. The symbols give the mean ratio of CR-to-total pressure in each spherical bin. It can be seen that the CR pressure is most relevant in the central regions, being comparable to the thermal pressure for $r < 50 h^{-1} \text{kpc}$ at all three epochs considered. At $z = 0$ and inside $100 h^{-1} \text{kpc}$, the mean CR pressure contributes about 37% of the total pressure for a spectral slope of $\alpha = 2.1$ (for the case of $\alpha = 2.4$ this number is $\sim 23\%$), while at the virial radius, the non-thermal pressure support drops to 14% (or 10% for $\alpha = 2.4$). Recall however that in this study we have excluded other potential sources of CRs, namely supernovae and cosmic structure formation shocks. They are expected to further increase the overall CR pressure content, and may also affect the relative contributions of non-thermal to thermal pressure as a function of radius (for further details on these issues see Pfrommer et al., 2007). Interestingly, given that the CR pressure contribution is comparable to the thermal pressure and that the CR pressure gradient is negative, the central cluster gas might be convectively unstable as proposed by Chandran & Dennis (2006) and explored in the case of SNe injected CRs by Pfrommer et al. (2007). Actually, since most of the CR pressure is due to CRs residing in the buoyantly rising bubbles, one can argue that the system indeed exhibits a CR-driven convection. An instability did not need to develop, since the CRs in the ICM are directly injected into an unstable configuration of a bubble.

The total X-ray luminosity within the virial radius in the case of CR bubbles with $\alpha = 2.4$ lies in between the

simulations performed without AGN feedback and the run with thermal bubbles. This increase of the X-ray emission is a result of the substantial Coulomb losses of the CR population combined with the softer equation state of the gas supported by non-thermal pressure. In the run with $\alpha = 2.1$, Coulomb losses are less important and the total X-ray luminosity is reduced from a value of $\sim 1.6 \times 10^{43} \text{ erg/s}$ for the case without AGN feedback to $\sim 9.2 \times 10^{42} \text{ erg/s}$. Also, in the simulation with $\alpha = 2.1$, the mean mass-weighted gas temperature is reduced, from 1.20 keV to 0.97 keV, indicating that CR bubbles may significantly influence galaxy cluster scaling relations such as the $L_X - T$ relationship, especially at the low mass end. We plan to analyze this question in more detail in a forthcoming study. Finally, we note that the bulk of the BH growth is not affected much by the presence of a non-thermal component in the bubbles: the BH growth is moderately reduced for $z < 2$, so that the most massive BH in the simulated volume has its mass reduced by less than 20% at $z = 0$. We also note that in our model the central star formation rate and the total stellar mass within R_{vir} (see below) are not very sensitive to whether the bubbles are filled with thermal or non-thermal energy, indicating that feedback by CR bubbles is about equally efficient in suppressing star formation in central galaxies as thermal ones.

4.2.2 Baryon fraction and AGN-driven bubbles

In the left-hand panel of Figure 6, we show the gas fraction at $z = 0$ within a given radius as a function of distance from the cluster centre. The radius has been normalized to R_{200} and the gas fraction is in units of the universal baryon fraction adopted in our simulation (i.e. $\Omega_b/\Omega_0 = 0.13$). The black line is for the run without AGN feedback, the blue line is for thermal bubbles, while the green ($\alpha = 2.4$) and red ($\alpha = 2.1$) lines show the case of CR bubbles. As a generic feature of AGN feedback, it can be seen that the gas fraction is significantly reduced in the central cluster region, while it is increased in the cluster outskirts. As expected, the central gas fraction is most suppressed in the simulation where the CR bubbles have a shallow momentum spectrum. On the other hand, the case with $\alpha = 2.4$ leads to a somewhat higher gas fraction with respect to the simulation with purely thermal bubbles, due to the combined effects of stronger Coulomb cooling and higher gas compressibility.

In the right-hand panel of Figure 6, we show the total baryon fraction (solid lines), and the stellar fraction (dashed lines) as a function of radius, using the same colour-coding. The amount of stars that form in the central regions is significantly reduced by the presence of a supermassive BH, but it is not affected by the nature of the bubbles, as discussed above. The total amount of stars drops from a high value in excess of $\sim 30\%$ reached in the simulation without AGN heating to a much more realistic value of $\sim 10\%$, which is consistent with observational findings (Lin et al., 2003). This also endows the central galaxy with a much redder colour, as observed. Due to the reduction of the central stellar fraction the total baryon fraction is lowered in the central regions as well. Only at radii comparable to the turnaround radius, at $\sim 3 \times R_{200}$, it reaches the universal value in all runs performed.

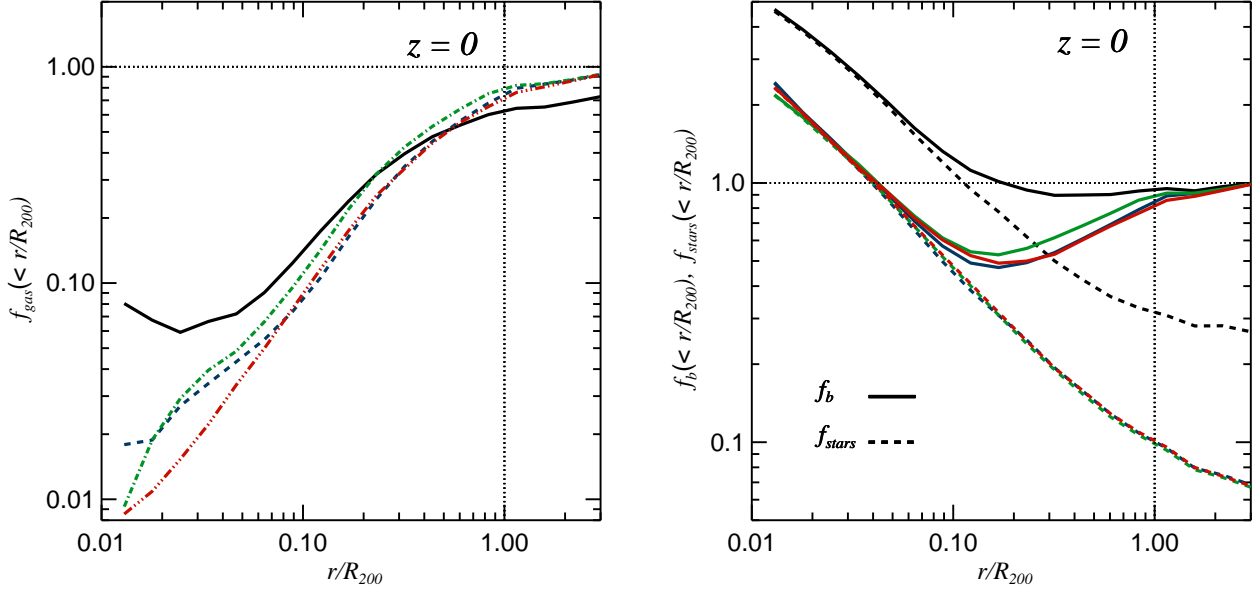


Figure 6. The left-hand panel shows the profile of the cumulative gas mass fraction as a function of radius at $z = 0$. The baryon fractions have been normalized to the universal value assumed in our simulations, i.e. 0.13. The black solid line is for the simulation with cooling and star formation only, while the remaining lines illustrate results for different runs with AGN feedback: thermal bubbles (blue dashed line), or bubbles filled with CRs (green dot-dashed for $\alpha = 2.4$, and red triple dot-dashed for $\alpha = 2.1$). The right-hand panel shows the total baryon mass fraction (solid lines) and the stellar mass fraction (dashed lines) with the same colour-coding.

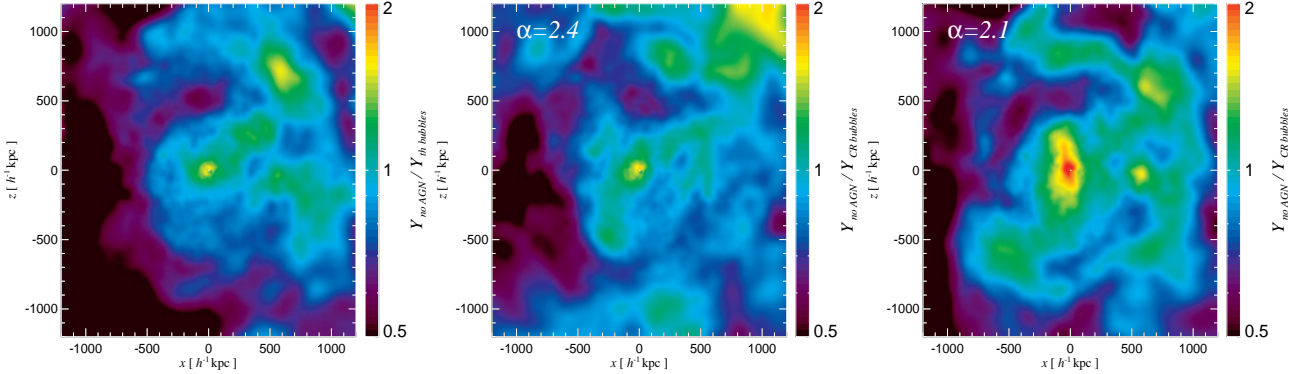


Figure 7. Ratio of the Compton- y parameters in our simulations without AGN feedback and in runs with AGN-driven bubbles at $z = 0$. The left-hand panel shows the case of thermal bubbles, the central panel that of CR bubbles with $\alpha = 2.4$, and the right-hand panel the case of CR bubbles with a steeper spectral index of $\alpha = 2.1$. It can be seen that the Compton- y parameter is decreased in the central regions due to the bubbles in all runs considered. However, in the cluster outskirts the bubbles tend to increase the Compton- y parameter, such that the area-integrated Comptonization can be both lower or higher than in the runs without AGN feedback.

4.2.3 Thermal SZ effect

Given that CRs provide a significant pressure support in the central cluster regions it is interesting to examine how they affect the amplitude of the thermal Sunyaev-Zel'dovich effect[†]. In Figure 7, we plot the ratio of the Compton- y pa-

[†] Note that we do not need to consider relativistic corrections to the pure thermal Sunyaev-Zel'dovich effect, given that we have modelled only CR protons. For a comprehensive study of non-thermal bubble imprints on the Sunyaev-Zel'dovich effect see e.g. Pfrommer et al. (2005).

rameter between the runs with and without AGN feedback at $z = 0$. The left-hand panel illustrates the case where bubbles are purely thermal, while the central ($\alpha = 2.4$) and right-hand panels ($\alpha = 2.1$) refer to the runs with CR bubbles. The Compton- y parameter is essentially determined by the line-of-sight integral of the thermal pressure. Since AGN-driven bubbles modify the thermal pressure distribution within the cluster, we observe variations of the estimated Compton- y parameter. More specifically, the Compton- y parameter is significantly reduced in the central cluster regions for all three runs with AGN feedback.

As a side effect of solving the overcooling problem, the self-regulated AGN feedback results in a lower central density that is in better agreement with the density profiles derived from X-ray measurements. In the cluster outskirts, however, the thermal pressure is somewhat increased in the runs with AGN feedback. This implies that the gas pressure distribution is somewhat “puffed up” in the cluster outskirts, which compensates for central gas depletion. Given that the thermal energy of the cluster is roughly constant and independent of the presence or absence of AGN heating, the area integrated Compton- y parameter turns out to be quite robust and is not changed much. It is primarily a measure of the cluster’s gravitational potential.

Still, this balance is not perfect as can be deduced by calculating the total Compton- y parameter Y within R_{vir} . In the case of thermal bubbles, we find that the integrated Compton- y parameter is increased by $\sim 10\%$, while in the case of CR bubbles with spectral index of 2.4 this number is somewhat smaller, being of order 7%. Interestingly, in the case of CR bubbles with a flatter spectral slope the total Compton- y parameter is instead lowered by $\sim 7\%$, as a result of a substantial reduction of the thermal pressure in the innermost regions. These results indicate that the integrated Comptonization is sensitive at a level of $\sim 10\%$ to the nature of AGN-driven bubbles and to the adopted feedback efficiency. This suggests that the presence of AGN feedback contributes to the scatter in the scaling relation between the cluster mass and Y , and the magnitude of this effect depends on the detailed physics of the AGN feedback. Further studies are needed to characterize the functional form of the scatter and to quantify a possible mass dependence of this effect. It is clear that the intended use of Y -measurements for high precision cosmology with galaxy clusters will require an accurate understanding of the detailed physical properties of AGN-inflated bubbles.

5 DISCUSSION

In this study we have investigated a model for self-regulated BH feedback with non-thermal relativistic particles in AGN-inflated bubbles. To describe the cosmic ray particles, we have adopted the formalism developed by Enßlin et al. (2007) and Jubelgas et al. (2008) for the treatment of CR protons, and combined it with prescriptions for BH growth and feedback, outlined in Springel et al. (2005) and Sijacki et al. (2007). This allowed us to study the influence of CR bubbles on their host clusters in self-consistent cosmological simulations of galaxy cluster formation, and in particular, to compare with the case where the bubbles are filled with purely thermal gas. Our methods also allowed us to gain some insight on how strongly the bubble morphologies and their propagation through the cluster atmosphere are affected by a cluster’s dynamical state and the gaseous bulk motions in the ICM.

We have found that simulations with CR bubbles much more faithfully resemble observational findings compared with the results for thermal bubbles. This is mostly driven by the softer equation of state of gas that is supported by non-thermal pressure, and by the longer dissipation timescale of the CR component relative to thermal cooling. As a result, CR bubbles can rise to the cluster outskirts and even

leak into the surrounding intergalactic medium. Still, their pressure support becomes gradually less important as they move away from cluster central regions. We have also found that the bubble morphologies in forming clusters are rather complex, especially during major merger events, where bubbles can become significantly perturbed from their initially spherical shape and are displaced from their initial injection axis. This implies that based on the spatial position of bubbles alone it is not readily possible to infer whether the AGN jet has changed its orientation between two successive outbursts or whether bulk motions in the ICM have displaced buoyantly rising bubbles.

Interestingly, we have found in our cosmological simulations that neither the BHARs nor the SFRs are very sensitive to the nature of the bubble feedback. However, the temperature distribution in the ICM is affected noticeably, given that CR bubbles provide non-thermal pressure support in central cluster regions. Above all, this changes the galaxy cluster temperature profiles which decline towards the innermost regions, being in much better agreement with the observed temperature profiles of cool core clusters. Correspondingly, the thermal pressure distribution is altered as well by CR bubbles, with a reduction of the thermal pressure in the centre and an increase in the outskirts. This redistribution of the thermal pressure can modify the integrated Compton- y parameter at a level of $\sim 10\%$, an effect that we expect to contribute to the scatter in the relationship between cluster mass and Y .

We have evaluated how many significant bubble outburst the central BH in our cluster is undergoing during the time interval from $z = 2$ to $z = 0$, when the BH is in the low accretion, ‘radio-mode’ regime. Based on this we obtain an average duty cycle of $\sim 10^8$ yrs. We note however that sudden inflows of gas towards the central BH triggered by merging activity – especially at $z = 0.6$, which corresponds to the last major merger of the host cluster – can cause much more frequent bubble events than the average value during a limited period. There is hence considerable variability in the duty cycle related to the merger history of the host halo, an issue we plan to investigate in more detail in a forthcoming study.

In our simulations, the sizes of the bubbles are not determined by calculating the jet physics from first principles, given that we cannot resolve the initial stage of jet formation and bubble inflation by a jet even in the most advanced state-of-art cosmological simulations. Instead, we rely on simple physical parameterizations and observational guidance to inject the bubbles with plausible sizes. Certainly this is an important limitation of our work and may in part be responsible for the rather large bubble sizes of up to a few hundred kpc that we find in some cases. On the other hand, there are two additional factors that may favor rather large bubble dimensions in our current modelling. One is that we have kept the injection axis constant with time. In some cases, the bubble injection time matches the buoyant rise time in such a way that fresh CR protons are injected into an already existing bubbles, making them reach a larger size. If this is also realized in nature, it is potentially ambiguous whether large bubbles are created by particularly powerful outbursts or result from several smaller outbursts which combine together.

However, we note that if CR diffusion is efficient (which

we have not considered in this study) it would be less probable that several bubble outbursts mix together into a large X-ray cavity. In this case an old bubble would already disperse before a new one could have time to reach it and combine with it. CR diffusion would also reduce the probability of finding a bubble at large enough distance from the cluster centre (and would also possibly modify the heating rates), thus more sophisticated studies and more stringent observational constraints are needed to pin-down the relevance of CR diffusion out of the bubbles.

The second factor which may bias the sizes of our simulated CR bubbles high is the fact that observationally only relativistic electrons have been detected so far in radio lobes, while we have conjectured in our simulations that there should be a spatially extended distribution of CR protons as well. Many of our CR bubbles, especially the ones that are further away from the central AGN, are expected to have a rather aged population of CR electrons, which would not have detectable radio emission. In our picture these bubbles correspond to the so-called ghost cavities which are identified as depressions in X-ray emission without any notable radio emission, or only radio emission at lower frequencies. Because of the very low contrast in projected surface brightness maps, many of these ghost cavities are missed both in observations and simulations. It will be an important task for future work to better quantify this bias, and to find powerful observational constraints for the relative content of relativistic electrons and protons in AGN-inflated bubbles. Our simulations certainly suggest that CRs may play a crucial role in shaping the central ICM properties and in regulating AGN activity in clusters of galaxies.

ACKNOWLEDGEMENTS

We are grateful to Simon White and Lars Hernquist for very helpful discussions and comments on this work. DS acknowledges the PhD fellowship of the International Max Planck Research School in Astrophysics, and a Postdoctoral Fellowship from the UK Science and Technology Funding Council (STFC).

REFERENCES

- Allen S. W., Dunn R. J. H., Fabian A. C., Taylor G. B., Reynolds C. S., 2006, *MNRAS*, 372, 21
- Birzan L., Rafferty D. A., McNamara B. R., Wise M. W., Nulsen P. E. J., 2004, *ApJ*, 607, 800
- Blanton E. L., Sarazin C. L., McNamara B. R., Wise M. W., 2001, *ApJ*, 558, L15
- Boehringer H., Morfill G. E., 1988, *ApJ*, 330, 609
- Bondi H., 1952, *MNRAS*, 112, 195
- Bondi H., Hoyle F., 1944, *MNRAS*, 104, 273
- Brüggen M., Kaiser C. R., 2002, *Nature*, 418, 301
- Chandran B. D., Dennis T. J., 2006, *ApJ*, 642, 140
- Churazov E., Brüggen M., Kaiser C. R., Böhringer H., Forman W., 2001, *ApJ*, 554, 261
- Churazov E., Forman W., Vikhlinin A., Tremaine S., Gerhard O., Jones C., 2007, *MNRAS* submitted, astro-ph/0711.4686
- Clarke T. E., Sarazin C. L., Blanton E. L., Neumann D. M., Kassim N. E., 2005, *ApJ*, 625, 748
- Dalla Vecchia C., Bower R. G., Theuns T., Balogh M. L., Mazzotta P., Frenk C. S., 2004, *MNRAS*, 355, 995
- Di Matteo T., Springel V., Hernquist L., 2005, *Nature*, 433, 604
- Dolag K., 2004, in *The Riddle of Cooling Flows in Galaxies and Clusters of galaxies*, edited by T. H. Reiprich, J. C. Kempner, N. Soker, 27–30, to be published electronically at <http://www.astro.virginia.edu/coolflow/>
- Dunn R. J. H., Fabian A. C., Taylor G. B., 2005, *MNRAS*, 364, 1343
- Enßlin T. A., Pfrommer C., Springel V., Jubelgas M., 2007, *A&A*, 473, 41
- Fabian A. C., Sanders J. S., Taylor G. B., Allen S. W., Crawford C. S., Johnstone R. M., Iwasawa K., 2006, *MNRAS*, 366, 417
- Forman W., et al., 2007, *ApJ*, 665, 1057
- Gould R. J., 1972, *Physica*, 58, 379
- Guo F., Oh S. P., 2008, *MNRAS*, 384, 251
- Hoyle F., Lyttleton R. A., 1939, in *Proceedings of the Cambridge Philosophical Society*, vol. 35 of *Proceedings of the Cambridge Philosophical Society*, 405–+
- Jenkins A., Frenk C. S., White S. D. M., Colberg J. M., Cole S., Evrard A. E., Couchman H. M. P., Yoshida N., 2001, *MNRAS*, 321, 372
- Jubelgas M., Springel V., Enßlin T., Pfrommer C., 2008, *A&A*, 481, 33
- Katz N., Weinberg D. H., Hernquist L., 1996, *ApJS*, 105, 19
- Lin Y.-T., Mohr J. J., Stanford S. A., 2003, *ApJ*, 591, 749
- Loewenstein M., Zweibel E. G., Begelman M. C., 1991, *ApJ*, 377, 392
- Mathews W. G., Brighenti F., 2007, *ApJ*, 660, 1137
- Mazzotta P., Kaastra J. S., Paerels F. B., Ferrigno C., Colafrancesco S., Mewe R., Forman W. R., 2002, *ApJ*, 567, L37
- McNamara B. R., Nulsen P. E. J., Wise M. W., Rafferty D. A., Carilli C., Sarazin C. L., Blanton E. L., 2005, *Nature*, 433, 45
- Miniati F., 2002, *MNRAS*, 337, 199
- Miniati F., Ryu D., Kang H., Jones T. W., 2001, *ApJ*, 559, 59
- Navarro J. F., Frenk C. S., White S. D. M., 1996, *ApJ*, 462, 563
- Navarro J. F., Frenk C. S., White S. D. M., 1997, *ApJ*, 490, 493
- Nulsen P. E. J., McNamara B. R., Wise M. W., David L. P., 2005, *ApJ*, 628, 629
- Omma H., Binney J., Bryan G., Slyz A., 2004, *MNRAS*, 348, 1105
- Owen F. N., Eilek J. A., Kassim N. E., 2000, *ApJ*, 543, 611
- Pfrommer C., 2008, *MNRAS*, 385, 1242
- Pfrommer C., Enßlin T. A., Sarazin C. L., 2005, *A&A*, 430, 799
- Pfrommer C., Enßlin T. A., Springel V., 2008, *MNRAS*, 385, 1211
- Pfrommer C., Enßlin T. A., Springel V., Jubelgas M., Dolag K., 2007, *MNRAS*, 378, 385
- Pfrommer C., Springel V., Enßlin T. A., Jubelgas M., 2006, *MNRAS*, 367, 113
- Quilis V., Bower R. G., Balogh M. L., 2001, *MNRAS*, 328, 1091
- Ruszkowski M., Begelman M. C., 2002, *ApJ*, 581, 223
- Ruszkowski M., Enßlin T. A., Brüggen M., Begelman M. C., Churazov E., 2008, *MNRAS*, 383, 1359
- Ryu D., Kang H., 2004, *Journal of Korean Astronomical Society*, 37, 477
- Ryu D., Kang H., Hallman E., Jones T. W., 2003, *ApJ*, 593, 599
- Sanders J. S., Fabian A. C., 2007, *MNRAS*, 381, 1381
- Sanderson A. J. R., Ponman T. J., O’Sullivan E., 2006, *MNRAS*, 372, 1496
- Schmidt R. W., Fabian A. C., Sanders J. S., 2002, *MNRAS*, 337, 71
- Sijacki D., Springel V., 2006a, *MNRAS*, 366, 397
- Sijacki D., Springel V., 2006b, *MNRAS*, 371, 1025
- Sijacki D., Springel V., di Matteo T., Hernquist L., 2007, *MNRAS*, 380, 877
- Simionescu A., Werner N., Finoguenov A., Böhringer H., Brüggen M., 2008, *A&A*, 482, 97
- Springel V., 2005, *MNRAS*, 364, 1105
- Springel V., Di Matteo T., Hernquist L., 2005, *MNRAS*, 361, 776
- Springel V., Hernquist L., 2002, *MNRAS*, 333, 649
- Springel V., Hernquist L., 2003, *MNRAS*, 339, 289

- Springel V., Yoshida N., White S. D. M., 2001, *New Astronomy*,
6, 79
Tormen G., Bouchet F. R., White S. D. M., 1997, *MNRAS*, 286,
865
Yoshida N., Sheth R. K., Diaferio A., 2001, *MNRAS*, 328, 669